ISSN (Print) 1226-1750
ISSN (Online) 2233-6656
Journal of Magnetics 19(2), 111-115 (2014) http://dx.doi.org/10.4283/JMAG.2014.19.2.111

Structural Phase Transition, Electronic Structure, and Magnetic Properties of Sol-gel-prepared Inverse-spinel Nickel-ferrites Thin Films

Kwang Joo Kim[1]*, Min Hwan Kim[1], and Chul Sung Kim[2]

[1]*Department of Physics, Konkuk University, Seoul 143-701, Korea*
[2]*Department of Physics, Kookmin University, Seoul 136-702, Korea*

(Received 7 February 2014, Received in final form 12 March 2014, Accepted 14 March 2014)

X-ray diffraction (XRD), X-ray photoelectron spectroscopy (XPS), and vibrating sample magnetometry (VSM) were used to investigate the influence of Ni ions on the structural, electronic, and magnetic properties of nickel-ferrites ($Ni_xFe_{3-x}O_4$). Spinel $Ni_xFe_{3-x}O_4$ ($x \leq 0.96$) samples were prepared as polycrystalline thin films on Al_2O_3 (0001) substrates, using a sol-gel method. XRD patterns of the nickel-ferrites indicate that as the Ni composition increases ($x > 0.3$), a structural phase transition takes place from cubic to tetragonal lattice. The XPS results imply that the Ni ions in $Ni_xFe_{3-x}O_4$ substitute for the octahedral sites of the spinel lattice, mostly with the ionic valence of +2. The minority-spin *d*-electrons of the Ni^{2+} ions are mainly distributed below the Fermi level (E_F), at around 3 eV; while those of the Fe^{2+} ions are distributed closer to E_F (~1 eV below E_F). The magnetic hysteresis curves of the $Ni_xFe_{3-x}O_4$ films measured by VSM show that as x increases, the saturation magnetization (M_s) linearly decreases. The decreasing trend is primarily attributable to the decrease in net spin magnetic moment, by the Ni^{2+} (2 μ_B) substitution for octahedral Fe^{2+} (4 μ_B) site.

Keywords: nickel-ferrite, spinel, phase transition, magnetization

1. Introduction

Iron-based ferrimagnetic oxides have drawn attention for decades, as a consequence of their wide range of engineering applications, as well as their interesting physical properties. Some of the ferrites are known to possess prominent magnetic and electrical properties, such as high saturation magnetization, high magnetic permeability, high electrical resistivity, and low power loss at high frequencies; these properties make them applicable for high-density magnetic recording, magnetic refrigeration, ferro-fluids, power transformers, and high-frequency microwave devices [1]. Magnetite (Fe_3O_4), a natural ferrimagnet, has frequently been adopted as a base material for developing particular ferrites, by cationic substitution in the tetrahedral (A) or octahedral (B) sites of the spinel lattice. Fe_3O_4 has the inverse-spinel structure, in which the A sites are occupied by Fe^{3+} ions, and the B sites are equally shared by Fe^{3+} and Fe^{2+} ions. Its ferrimagnetism below the Curie temperature ($T_C \sim 860$ K) has been explained in terms of the antiferromagnetic spin alignment between Fe^{3+}(A) and Fe^{3+}(B) ions, via the super-exchange interaction; while Fe^{2+}(B) aligns parallel to Fe^{3+}(B), via the double-exchange interaction. The high electrical conductivity of Fe_3O_4 (~10^2 $\Omega^{-1}cm^{-1}$ at room temperature) has been explained in terms of the polaronic electron hopping between Fe^{2+}(B) and Fe^{3+}(B) ions [2, 3]. Due to the half-metallic electronic structure of Fe_3O_4, the spin-polarized conduction electrons may be useful for realizing spin-transport devices [4, 5]. Ferrimagnetic oxides with high T_C, as well as good electrical conductivity, can be good candidates for such purposes.

In case some of the cations in magnetite are replaced by Ni ions, the resultant nickel-ferrites ($Ni_xFe_{3-x}O_4$) are likely to have structural, electrical and magnetic properties that evolve significantly from those of Fe_3O_4. The changes in those properties tend to be governed by the distribution of the cations among the A and B sites, which is likely to be mainly affected by the cationic radius and orbital preference. The cationic distribution in the spinel oxides may also be affected by sample preparation, for example single crystals, nanocrystalline powders, and thin films.

In the present work, phase-pure $Ni_xFe_{3-x}O_4$ thin films have been successfully synthesized on Al_2O_3 (0001) sub-

*Corresponding author: Tel: +82-2-450-3085
Fax: +82-2-3436-5361, e-mail: kjkim@konkuk.ac.kr

strates, using a solution growth technique, for Ni concentrations up to x = 0.96. Although the majority of research on ferrites tends to be focused on powder samples, film samples are more advantageous in studying the inherent properties, such as the electrical conductivity, optical absorption and photoelectron spectroscopy, of the granular ferrites. The structural, electronic, and magnetic properties of the nickel-ferrite films, as measured by using X-ray diffraction (XRD), X-ray photoelectron spectroscopy (XPS), and vibrating sample magnetometry (VSM), were analyzed, in comparison with those of magnetite.

2. Experimental Details

In the present sol-gel process, the precursor solution was prepared by first dissolving $Fe(NO_3)_3 \cdot 9H_2O$ powders in 2-methoxyethanol. Then, $Ni(CH_3CO_2)_2 \cdot 4H_2O$ powders were added, and stirred at 60 °C for 40 min. The substrates, Al_2O_3 (0001) wafers, were spin-coated with the precursor solution at 3000 rpm for 20 sec, and then heated at 160 and 250 °C for 3 min each after each deposition, in order to remove the organic substances. This process was repeated 10 times, and then annealing was performed on the precursor films at 750 °C for 5 h in vacuum (~10^{-3} Torr), to obtain the present $Ni_xFe_{3-x}O_4$ films. For the Fe_3O_4 sample, the annealing temperature and duration were 800 °C and 4 h. The film thicknesses of the samples were in the 400-500 nm range, which was confirmed by scanning electron microscopy.

The Ni:Fe ratio in the $Ni_xFe_{3-x}O_4$ films was determined by using energy-dispersive X-ray spectroscopy. The crystalline structure of the samples was examined by using XRD with the Cu K_α line in the grazing-incidence manner, with a fixed X-ray incidence angle of 4°. XPS measurements were performed using the Al K_α line on Fe 2*p*, Ni 2*p*, O 1*s*, and valence states of the ferrite samples, to find the preferred valences of the cations, and the *d*-electron distribution near the Fermi level. The magnetic hysteresis curves of the $Ni_xFe_{3-x}O_4$ films were measured at room temperature using VSM, with the magnetic field H (≤ 10 kOe) applied parallel to the plane of the film.

3. Results and Discussion

In Fig. 1(a), the XRD patterns of the polycrystalline $Ni_xFe_{3-x}O_4$ film samples measured at room temperature are compared with that of the Fe_3O_4 sample. For the x = 0.30 sample, all the diffraction peaks are well indexed based on the cubic spinel phase (space group $Fd\bar{3}m$), and are shifted to higher angles, compared to those of the Fe_3O_4 sample. This indicates that Ni doping caused a

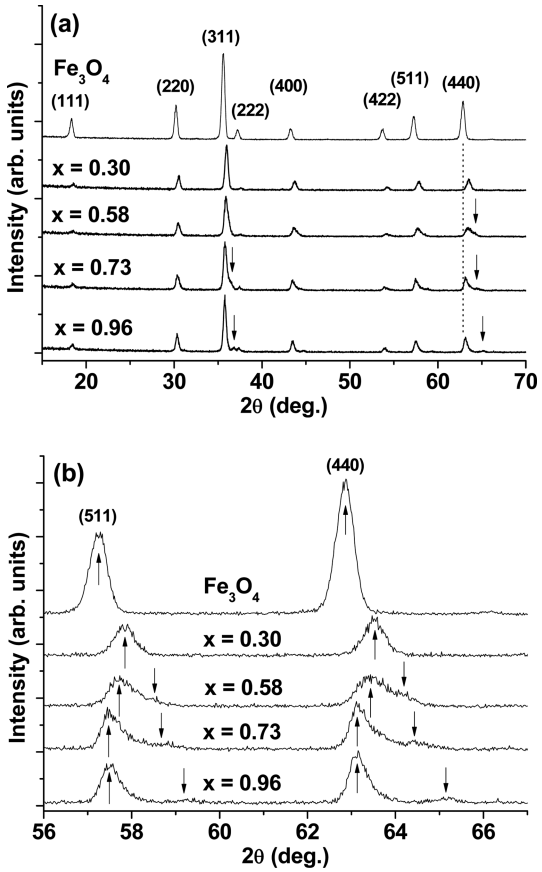

Fig. 1. (a) XRD patterns of polycrystalline $Ni_xFe_{3-x}O_4$ thin films, and (b) Magnified (511) and (440) peaks of the XRD patterns.

decrease of the lattice constant and the unit-cell volume. Also, new diffraction peaks appear for the samples with the higher Ni compositions, as marked by the arrows in Fig. 1(a). In Fig. 1(b), magnified (511) and (440) peaks for the $Ni_xFe_{3-x}O_4$ samples are compared with those of the Fe_3O_4 sample. For the samples with x = 0.58 and above, some of the peaks entail another peak at the higher angle, as marked by the arrows. Thus, the XRD patterns indicate that the $Ni_xFe_{3-x}O_4$ samples have a tetragonal structure for x = 0.58 and above; while they have a cubic structure for x = 0.30 and below. In Fig. 2, the lattice constants of the nickel-ferrite samples estimated from the shifts of the XRD peaks are exhibited, in comparison with that of the Fe_3O_4 sample. This indicates that the tetragonal distortion is gradually enhanced as the Ni composition increases in the nickel-ferrites, leading to a decrease in the unit-cell volume.

In Fig. 3(a), Fe 2*p*-electron binding-energy (BE) spectrum of the nickel-ferrite (x = 0.96) sample obtained from XPS measurements is compared with that of the Fe_3O_4 sample. The Fe 2*p*-electron spectra consist of spin-orbit-

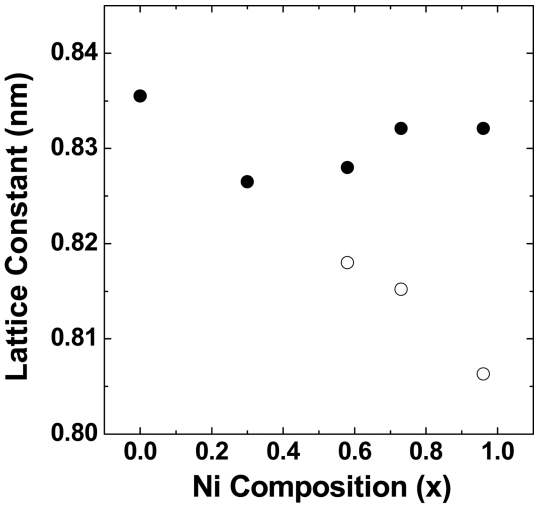

Fig. 2. Lattice constants of $Ni_xFe_{3-x}O_4$ films. Filled and open circles represent constants a and c, respectively. The unit-cell volume is a^3 for cubic, and a^2c for tetragonal structure.

split $2p_{3/2}$ and $2p_{1/2}$ peaks, and satellites that are sensitive to the spin state of the compound. The main $2p_{3/2}$ peak for the Fe_3O_4 sample is seen to be well resolved into two contributions, Fe^{2+} (BE~709 eV) and Fe^{3+} (BE~711 eV), separated by ~2 eV, as marked by the arrows in Fig. 3(a). The $2p$-electron spectral shapes for the present multi-valence iron oxides are well distinguishable from those for oxides containing Fe^{3+} ions only [6, 7]. For the x = 0.96 sample, the Fe^{3+} peak is seen to be dominant, compared to that of Fe_3O_4, suggesting significant reduction in Fe^{2+} density, caused by the Ni doping. The satellites around 719 and 733 eV are ascribed to the Fe^{3+} ions.

The Ni $2p$ XPS spectrum of the x = 0.96 sample is exhibited in Fig. 3(b). The spectrum exhibits sharp peaks near 855 eV ($2p_{3/2}$) and 873 eV ($2p_{1/2}$), with the energy difference (spin-orbit splitting) of 18 eV, suggesting that the Ni ions in nickel-ferrites mostly have a valence of +2. The peak near 862 eV, as marked by the asterisk (*), is identified as a major satellite to the $2p_{3/2}$ main line of Ni^{2+} ion [8, 9]. Considering the observed reduction of Fe^{2+} (709 eV) line intensity of the x = 0.96 sample, compared to that of the Fe_3O_4 sample, the dominance of the Ni^{2+} line implies that the Ni^{2+} ions substitute for the Fe^{2+}(B) sites in the $Ni_xFe_{3-x}O_4$ samples.

In Fig. 3(c), the XPS spectrum from the valence electrons of the x = 0.96 sample is compared with that of the Fe_3O_4 sample. The valence bands of the two oxides consist of the $3d$ electrons of Fe and Ni ions. The two

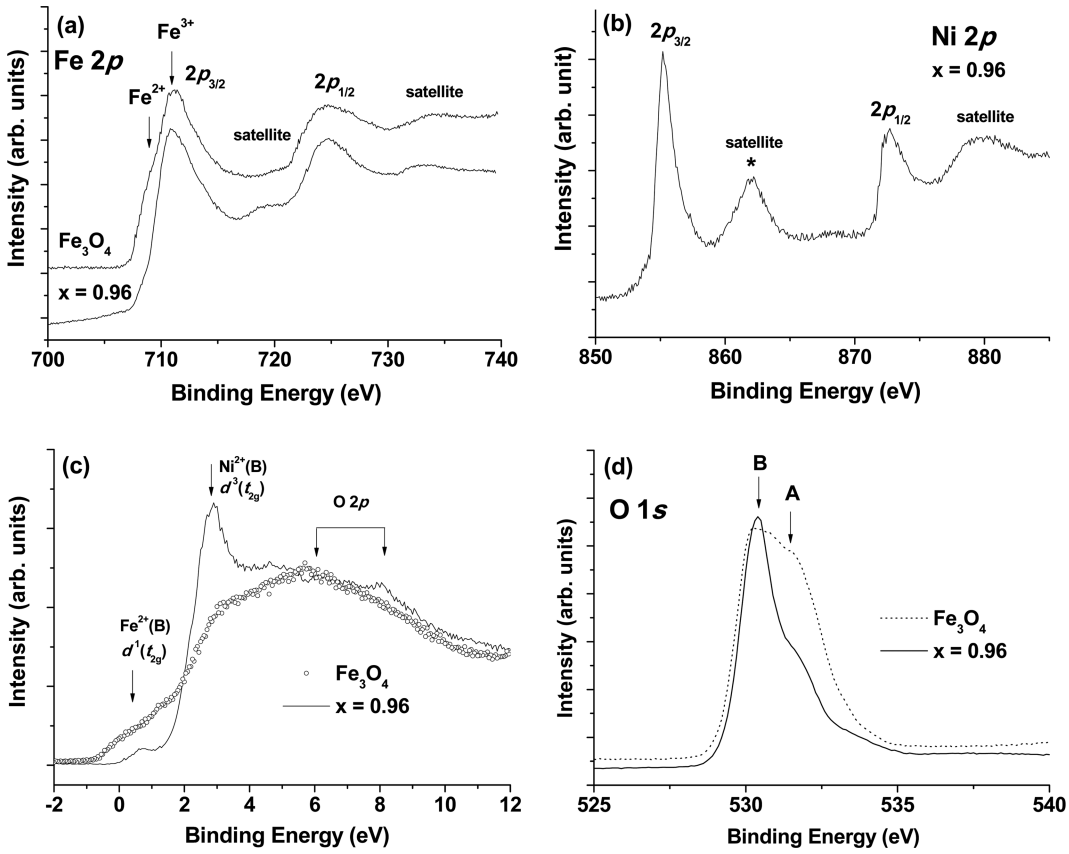

Fig. 3. X-ray photoelectron spectra of $Ni_xFe_{3-x}O_4$ films. (a) Fe $2p$, (b) Ni $2p$, (c) valence band, and (d) O $1s$ electrons.

XPS spectra exhibit difference in two regions: (i) near the Fermi level E_F (BE = 0), and (ii) well below E_F, near BE = 3 eV. The observed emission structure near E_F for the Fe_3O_4 sample is ascribed to minority-spin *d* electrons from the Fe^{2+}(B) ions. Theoretically, one of the d^6 electrons in the Fe^{2+}(B) ion in ferrimagnetic Fe_3O_4 occupies a minority-spin t_{2g} state that is located close to E_F; while the majority-spin *d* states are completely filled with five electrons. The minority-spin t_{2g}(B) electron is most likely to contribute to good electrical conductivity in magnetite. The near-Fermi-edge emission is seen to be greatly reduced for the XPS spectrum of the nickel-ferrite (x = 0.96) sample. On the other hand, the XPS spectrum of the nickel-ferrite sample exhibits a strong emission peak near BE = 3 eV, as shown in Fig. 3(c). The 3-eV peak is ascribed to the *d*-electrons of the Ni^{2+} ions. The minority-spin *d* states of the Ni^{2+}(d^8) ion, which are responsible for the 3-eV peak, are occupied by three t_{2g} electrons. Thus, the XPS data imply that Ni^{2+} ions mainly substitute for the Fe^{2+}(B) sites in the nickel-ferrite samples. Then, the A sites of the nickel-ferrites are likely to mostly be occupied by Fe^{3+} ions, exhibiting inverse-spinel nature. Such octahedral preference of Ni^{2+} ions was reported in a number of nickel-ferrite systems [10-12]. When Ni^{2+} ion subsists at the B site, its ionic radius is known to be about 0.083 nm, significantly smaller than that of the octahedral Fe^{2+} ion (0.092 nm) [13]. The cubic → tetragonal phase transition is attributable to the difference in bond angle and length between Fe-O-Fe and Ni-O-Fe in the B sites [14], derived from the difference in ionic radius. The observed reduction of the unit-cell volume of the nickel-ferrites, compared to that of Fe_3O_4 (Fig. 2), can be explained by the existence of the octahedral Ni^{2+} ions. The reduction of Fe^{2+}(B) density by the Ni^{2+} substitution can be used to explain the diminished electrical conductivity of nickel-ferrites [14] (~10^{-8} $\Omega^{-1}cm^{-1}$ at room temperature for x ~ 1), in terms of the reduced Fe^{2+}(B) → Fe^{3+}(B) electron hopping probability.

In Fig. 3(d), the O 1*s*-electron BE spectrum of the nickel-ferrite (x = 0.96) sample obtained from XPS measurements is compared with that of the magnetite sample. The peak near 530.5 eV (denoted as B) is ascribed to O^{2-} ions at the octahedral coordinates; while the peak near 531.5 eV (denoted as A) is ascribed to O^{2-} ions at the tetrahedral coordinates. The observed reduction in the strength of the peak A of the x = 0.96 sample, compared to that of the Fe_3O_4 sample, implies the formation of vacancies in the tetrahedral oxygen sites. The exposure of the film's surface to air in the spin-coating steps, and to vacuum during post-annealing, is likely to promote oxygen vacancies, due to oxygen out-diffusion from the surface

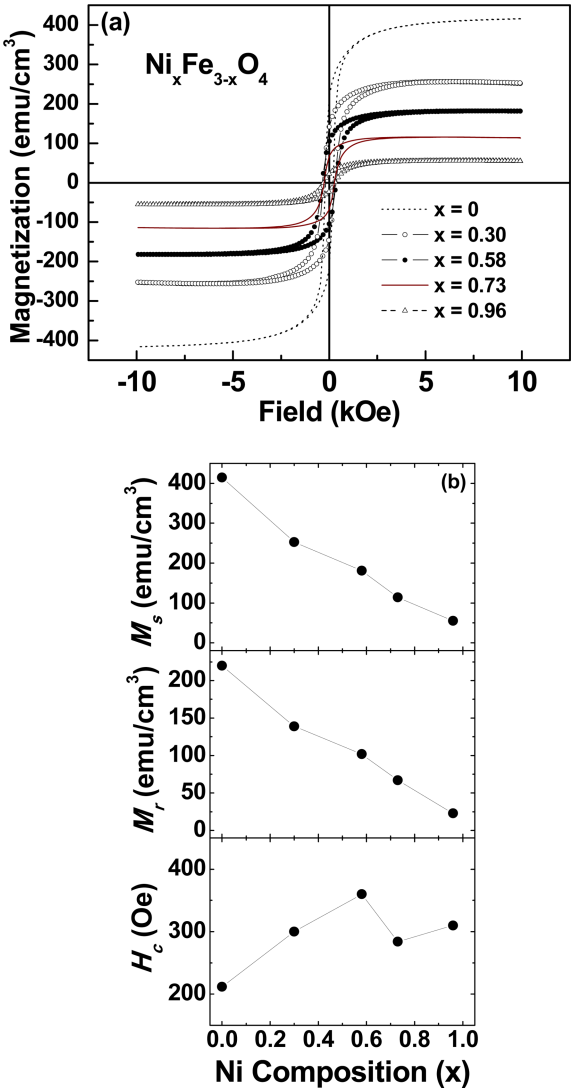

Fig. 4. (Color online) (a) *M-H* curves of $Ni_xFe_{3-x}O_4$ films measured at room temperature by using VSM. (b) Saturation magnetization (M_s), remanent magnetization (M_r), and coercivity (H_c) for $Ni_xFe_{3-x}O_4$ films, obtained from VSM plots.

[15].

Figure 4(a) exhibits the result of magnetic hysteresis (*M*) measurements on the $Ni_xFe_{3-x}O_4$ samples, using VSM at room temperature, under an external field (*H*) varying up to 10 kOe. All the samples exhibit hysteresis behavior in the *M-H* curve, indicative of ferrimagnetism in $Ni_xFe_{3-x}O_4$. Figure 4(b) exhibits the saturation magnetization (M_s), remanent magnetization (M_r), and coercivity (H_c) of the samples obtained from the hysteresis plots. It is seen that with increasing x, M_s and M_r exhibit a decreasing trend in a linear manner. With the magnetic moment of Fe ion in the A sites being opposite that of the Fe ion in the B sites, Fe_3O_4 has a theoretical net spin magnetic moment of 4 μ_B per formula unit (= 500 emu/cm^3), at temperatures below

T_C. The observed M_s for the Fe_3O_4 sample is ~80% of the theoretical value. Thus, the monotonic decreasing trend of M_s and M_r can be understood in terms of the substitution of Ni^{2+} ions for the Fe^{2+}(B) sites. The spin magnetic moment of a high-spin $Ni^{2+}(d^8)$ ion is 2 μ_B, which is a half of that of $Fe^{2+}(d^6)$ ion (4 μ_B). The smaller M_s of the $Ni_xFe_{3-x}O_4$ samples, compared to the theoretically expected value (e.g. the theoretically expected value of M_s for the x = 0.96 sample is ~200 emu/cm^3 (~50% of that of Fe_3O_4), while the observed value is only 55 emu/cm^3) is attributable to a weakening of the Fe^{3+}(A)-Fe^{3+}(B) super-exchange interaction, due to the oxygen vacancies.

4. Conclusions

Inverse-spinel $Ni_xFe_{3-x}O_4$ thin-film ferrites prepared by a sol-gel process on Al_2O_3 (0001) substrates exhibit cubic → tetragonal phase transition, with increase of Ni content. The XPS results suggest that Ni^{2+} ions mainly substitute for Fe^{2+}(B) sites in the nickel-ferrites. The observed decrease in the unit-cell volume with increasing Ni content can be explained in terms of the smaller ionic radius of Ni^{2+}(B) ion, compared to that of Fe^{2+}(B) ion. The Ni^{2+}(B) ion has minority-spin *d*-electrons having greater binding energies by ~2 eV, than those of the Fe^{2+}(B) ion. The decrease in M_s and M_r of the nickel-ferrite films with increase of Ni content can be explained by comparing the spin magnetic moment of the octahedral Ni^{2+} ion (2 μ_B), with that of Fe^{2+} ion (4 μ_B).

Acknowledgment

This work was supported by Konkuk University, in the 2013 program year.

References

[1] A. Goldman, Modern Ferrite Technology, 2nd ed., Springer, New York, 2006.
[2] S. B. Ogale, K. Ghosh, R. P. Sharma, R. L. Greene, R. Ramesh and T. Venkatesan, Phys. Rev. B **57**, 7823 (1998).
[3] K. J. Kim, T. Y. Koh, C. S. Kim, and Y. B. Lee, J. Korean Phys. Soc. **64**, 93 (2014).
[4] Y. S. Dedkov, U. Rudiger, and G. Guntherodt, Phys. Rev. B **65**, 064417 (2002).
[5] W. Wang, M. Yu, M. Batzill, J. He, U. Diebold, and J. Tang. Phys. Rev. B **73**, 134412 (2006).
[6] T. Fujii, F. M. F. de Groot, G. A. Sawatzky, F. C. Voogt, T. Hibma, and K. Okada, Phys. Rev. B **59**, 3195 (1999).
[7] K. J. Kim, J. H. Lee, and C. S. Kim, J. Korean Phys. Soc. **61**, 1274 (2012).
[8] S. Altieri, L. H. Tjeng, A. Tanaka, and G. A. Sawatzky, Phys. Rev. B **61**, 13403 (2000).
[9] S. Ivanova, E. Zhecheva, R. Stoyanova, D. Nihtianova, S. Wegner, P. Tzvetkova, and S. Simova, J. Phys. Chem. C **115**, 25170 (2011).
[10] A. K. Singh, T. C. Goel, and R. G. Mendiratta, Solid State Commun. **125**, 121 (2003).
[11] M. Sertkol, Y. Koseoglu, A. Baykal, H. Kavas, and A. C. Basaran, J. Magn. Magn. Mater. **321**, 157 (2009).
[12] P. Sivakumar, R. Ramesh, A. Ramanand, S. Ponnusamy, and C. Muthamizhchelvan, J. Alloys Compd. **563**, 6 (2013).
[13] R. D. Shannon, Acta Crystallogr., Sect. A **32**, 751 (1976).
[14] S. S. R. Inbanathan, V. Vaithyanathan, J. A. Chelvane, G. Markandeyulu, and K. K. Bharathi, J. Magn. Magn. Mater. **353**, 41 (2014).
[15] P. D. Thang, G. Rijnders and D. H. A. Blank, J. Magn. Magn. Mater. **310**, 2621 (2007).